

RESEARCH

Open Access



Dual-region MRI radiomic analysis indicates increased risk in high-risk breast lesions: bridging intratumoral and peritumoral radiomics for precision decision-making

Yuting Yang¹, Tingting Liao¹, Xiao-Hui Lin¹, Rushan Ouyang², Qiu Chen³ and Jie Ma^{1*}

Abstract

Objective To evaluate the clinical utility of dynamic contrast-enhanced magnetic resonance imaging (DCE-MRI)-derived clinicoradiological characteristics and intratumoral/peritumoral radiomic features in predicting pathological upgrades (malignant transformation) in high-risk breast lesions.

Materials and methods Retrospectively collected the data of 174 patients with high-risk breast lesions who underwent preoperative breast MRI examinations and were confirmed by biopsy pathology in Shenzhen People's Hospital between January 1, 2019 and January 1, 2024. The dataset was randomly divided into a training set ($n=121$) and a test set ($n=53$) at a ratio of 7:3. Initially, during the second stage of DCE-MRI, the region of interest (ROI) was delineated along the maximum cross-section of the lesion, and then automatically expanded outward by 3 mm, 5 mm, and 7 mm as the peritumoral ROIs. The intratumoral, each peritumoral, and the combined intratumoral and peritumoral radiomic models were established respectively. Independent risk factors predictive of malignant upgrades in high-risk lesions were identified through univariate and multivariable logistic regression analyses, which were subsequently incorporated as clinical and imaging characteristics. Finally, a combined model was established by integrating the intratumoral and peritumoral radiomic features with the clinical and imaging features. The performance of each model was analyzed using the receiver operating characteristic (ROC) curves, and the area under the curve (AUC) was calculated.

Results The peritumoral 3 mm radiomics model achieved the highest diagnostic performance among all the peritumoral models, with the AUC values of 0.704 and 0.654 for the training and test sets, respectively. In the training set, the combined model showed the highest diagnostic performance (AUC = 0.883), which was superior to that of the clinical and imaging features model (AUC = 0.745, $P=0.003$), the intratumoral radiomics model (AUC = 0.791, $P=0.027$), the peritumoral 3 mm radiomics model (AUC = 0.704, $P=0.001$), and the combined intratumoral and peritumoral radiomic model (AUC = 0.830, $P=0.004$). In the test set, the combined model also showed the highest diagnostic performance (AUC = 0.851). The combined model constructed by integrating the intratumoral and peritumoral radiomics features with the clinical and imaging features had the best diagnostic performance, with the

*Correspondence:

Jie Ma
cjr.majie@vip.163.com

Full list of author information is available at the end of the article



© The Author(s) 2025. **Open Access** This article is licensed under a Creative Commons Attribution-NonCommercial-NoDerivatives 4.0 International License, which permits any non-commercial use, sharing, distribution and reproduction in any medium or format, as long as you give appropriate credit to the original author(s) and the source, provide a link to the Creative Commons licence, and indicate if you modified the licensed material. You do not have permission under this licence to share adapted material derived from this article or parts of it. The images or other third party material in this article are included in the article's Creative Commons licence, unless indicated otherwise in a credit line to the material. If material is not included in the article's Creative Commons licence and your intended use is not permitted by statutory regulation or exceeds the permitted use, you will need to obtain permission directly from the copyright holder. To view a copy of this licence, visit <http://creativecommons.org/licenses/by-nc-nd/4.0/>.

sensitivity, specificity, and accuracy of 79.4%, 82.7%, and 81.8% in the training set, and 72.7%, 85.7%, and 83.0% in the test set, respectively.

Conclusion The combined predictive model, which integrates intratumoral and peritumoral radiomic features with clinical and imaging data, exhibited strong diagnostic performance and a clinically applicable nomogram was constructed to stratify individualized upgrade risk, assisting clinicians in making more precise decisions.

Keywords High-risk lesions, Radiomics, Dynamic magnetic resonance imaging, Peritumoral

Introduction

According to the 2024 global cancer statistics released by the World Health Organization's International Agency for Research on Cancer (IARC) [1], breast cancer currently ranks first in global female cancer incidence. Early precise diagnosis and risk stratification of breast cancer are crucial for improving patient outcomes. The European Quality Assurance Guidelines for Breast Cancer Screening and Diagnosis [2] classify breast biopsy pathology into five categories (B1-B5) based on lesion type and risk level, where B3 denotes high-risk lesions. High-risk lesions include atypical ductal hyperplasia (ADH), papillary lesions, complex sclerosing adenosis, mucinous neoplasms, and flat epithelial atypia.

High-risk breast lesions represent a biologically and clinically heterogeneous group with varying degrees of increased breast cancer risk. Literature statistics indicate that approximately 9.9–35.1% of high-risk lesions may progress to ductal carcinoma in situ (DCIS) or invasive ductal carcinoma (IDC) [3, 4]. Conventional breast magnetic resonance imaging (MRI) examinations demonstrate limited efficacy in differentiating malignant upgrades of postoperative high-risk breast lesions, frequently resulting in unnecessary biopsy procedures and therapeutic overtreatment. Therefore, there is an urgent need for non-invasive and high-precision prediction tools to optimize clinical decision-making pathways.

In recent years, radiomics has provided novel insights into deciphering the biological behavior of breast cancer through high-throughput extraction of quantitative features from both intratumoral and peritumoral regions [5–9]. Conversely, peritumoral microenvironmental characteristics correlate strongly with tumor aggressiveness and metastatic potential [10]. For instance, L. YB's team revealed that radiomic features from a 4-mm peritumoral zone achieved superior predictive performance for axillary lymph node metastasis in breast cancer (AUC=0.871) compared to conventional intratumoral models [11].

These findings suggest that integrating intratumoral and peritumoral MRI radiomic features could enable more comprehensive biological profiling of high-risk breast lesions, thereby enhancing predictive accuracy. While existing studies [12–15] typically define peritumoral regions as those 2–10 mm beyond the tumor

boundary, this study aims to develop a predictive model for high-risk lesion upgrading by synergizing optimal peritumoral MRI radiomics with intratumoral features and clinical-imaging biomarkers. Through deep mining of quantitative MRI signatures coupled with multimodal data integration, we seek to provide clinicians with an objective decision-support tool demonstrating improved diagnostic precision over conventional approaches.

Materials and methods

Study cohort

This study was conducted in accordance with the ethical principles of the Declaration of Helsinki and approved by the Institutional Review Board of Shenzhen People's Hospital (Approval No. LL-KY-2021624), with a waiver of informed consent due to its retrospective nature. We retrospectively reviewed the medical records of patients diagnosed with breast high-risk breast lesions (including ADH, papillary lesions, complex sclerosing adenosis, mucinous neoplasms, and flat epithelial atypia) at Shenzhen People's Hospital between January 1, 2019, and January 1, 2024.

Inclusion and exclusion criteria

The inclusion criteria were as follows: (1) histopathological confirmation of high-risk breast lesions via core needle biopsy; (2) no prior biopsy performed before the MRI examination; (3) availability of complete clinical documentation and standardized preoperative breast MRI protocols; (4) definitive postoperative histopathological diagnosis or comprehensive follow-up data (≥ 12 months). Cases were excluded if they met any of the following criteria: (1) technically inadequate MRI images precluding diagnostic analysis and ROI delineation; (2) non-enhancing lesions, lesions with indeterminate enhancement (defined as $< 10\%$ signal intensity increase on contrast-enhanced sequences), or lesions obscured by severe background parenchymal enhancement (BPE); (3) history of prior breast interventions, including biopsy, surgery, radiation therapy, chemotherapy, or hormonal therapy.

MRI imaging data acquisition

Breast MRI examinations were conducted using Siemens Skyra 3.0T and Avanto 1.5T scanners (Siemens

Healthineers, Germany) equipped with dedicated breast coils, with patients positioned prone and breasts naturally suspended. Non-contrast sequences included axial T1-weighted imaging (T1WI), T2-weighted imaging (T2WI) with fat suppression, and diffusion-weighted imaging (DWI) using the following parameters: TR=5700 ms, TE=59 ms, acquisition matrix=192×96, FOV=340 mm, slice thickness=4 mm, interslice gap=0.8 mm, 32 slices, and b-values of 50, 400, and 800 s/mm². Dynamic contrast-enhanced MRI (DCE-MRI) employed a 3D FLASH gradient-echo sequence with parameters set to TR=4.7 ms, TE=1.7 ms, slice thickness=1.6 mm, no interslice gap, 72 slices, acquisition matrix=448×372, FOV=360 mm, and flip angle=10°. The protocol initiated with a pre-contrast mask acquisition, followed by a 30-second pause during which gadopentetate dimeglumine (Gd-DTPA) was administered via power injector at 3 mL/s (dose: 0.1 mmol/kg body weight), followed by a 20 mL saline flush. Five consecutive post-contrast acquisitions were then performed at 1-minute intervals, yielding six total dynamic phases (including the mask) over a total scan duration of 6 min and 33 s. Patients were instructed to maintain strict immobility throughout the imaging session to minimize motion artifacts.

Radiomics analysis

Image ROI delineation

Prior studies indicate that the 60-120-second post-contrast phase (peak enhancement window for malignant lesions relative to the glandular background) is optimal for tumor characterization in breast MRI [16, 17]. Accordingly, this study selected the second-phase DCE-MRI images acquired at 120 s post-injection for

ROI delineation. All enrolled DCE-MRI datasets were retrieved from the Picture Archiving and Communication System (PACS) of Shenzhen People’s Hospital in DICOM format. The second-phase DCE-MRI images were imported into the Darwin Intelligent Research Platform (Yizhun Intelligent Technology Co., Ltd., Beijing, China) for analysis.

Two senior radiologists (each with >8 years of breast MRI diagnostic experience) independently performed blinded semi-automatic ROI delineation on the platform. All the ROIs were reviewed by a senior radiologist (15 years’ experience). Key steps included: the identification of the maximal cross-sectional area of the lesion on axial images. Semi-automatic 3D ROI delineation along lesion margins. Generation of peritumoral regions via automatic expansion algorithms at 3 mm, 5 mm, and 7 mm distances from the tumor boundary (Fig. 1). During ROI delineation, necrotic tumor regions were carefully avoided, and in cases where the predefined expansion distance exceeded the maximum anatomical clearance between the lesion periphery and adjacent structures (e.g., skin surface or chest wall), the peritumoral region was redefined as the spatial extent from the tumor boundary to the nearest anatomical boundary.

Radiomics feature extraction, preprocessing, and selection

Radiomic feature extraction was performed on the intratumoral and peritumoral ROIs using the Darwin Intelligent Research Platform (Yizhun Intelligent Technology Co., Ltd., Beijing, China). Extracted features encompassed three categories: morphological features, first-order statistical features, and texture features. Normalization was implemented via maximum absolute value scaling to mitigate feature magnitude disparities.

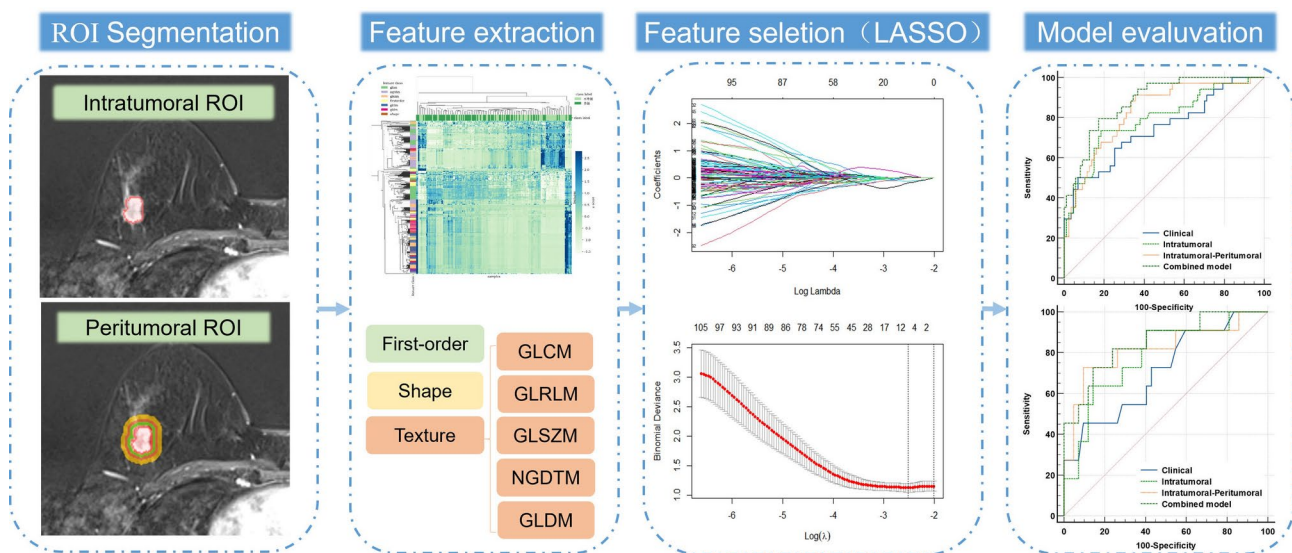


Fig. 1 The radiomics analysis workflow

The Least Absolute Shrinkage and Selection Operator (LASSO) regression algorithm was applied for multi-step feature selection, effectively eliminating redundant features while preserving those with strong discriminative power (Fig. 1). Radiomic features were separately extracted from intratumoral and peritumoral regions, including morphological features, first-order features, gray-level co-occurrence matrix (GLCM) features, gray-level size zone matrix (GLSZM) features, gray-level run-length matrix (GLRLM) features, gray-level dependence matrix (GLDM) features, neighboring gray tone difference matrix (NGTDM) features, LoG Sigma features, Wavelet features, and Local Binary Pattern (LBP) features. A total of 1,307 radiomic features were extracted in this study. Through LASSO regression analysis, 7 radiomic features were ultimately selected.

Patient cohort stratification and randomized allocation

Stratification by Pathology Type: The entire patient cohort was first stratified based on pathological classification. This preliminary stratification guaranteed proportional representation of each lesion category in both training and test sets.

Randomized Allocation within Strata: Within each pathological stratum, patients were randomly assigned to either the training set (70%) or testing set (30%) using a computer-generated random number sequence. This process was programmatically implemented to eliminate human selection bias.

Model development and validation

Logistic regression analysis was employed to construct four radiomic models based on optimally selected features: an intratumoral model, peritumoral models (3 mm, 5 mm, and 7 mm expansions), and a combined intratumoral-peritumoral model. Radiomic scores (Rad-scores) were derived for each model using weighted coefficients of the selected features. A clinical and imaging model was additionally developed using independent risk factors identified from clinical and imaging characteristics, with validation performed for independent cohort. ROC curves were plotted for the intratumoral model, individual peritumoral models, and the optimal combined intratumoral-peritumoral model. Comparative analyses of the AUC, accuracy, sensitivity, and specificity were conducted among the three peritumoral models. The peritumoral expansion radius demonstrating the highest predictive performance was integrated with intratumoral radiomic features to generate a combined radiomics model. Rad-scores from this model, along with univariate-selected clinical and imaging predictors, were subjected to multivariate logistic regression. Statistically significant variables were incorporated into a radiomic nomogram model. Calibration curves were generated

to assess the nomogram's predictive accuracy. We confirmed that the radiomics workflow strictly adhered to the Image Biomarker Standardization Initiative (IBSI) guidelines to ensure reproducibility across imaging platforms.

Statistical analysis

Statistical analyses were performed using SPSS 27.0 (IBM Corp., Armonk, NY) and R 4.3.2 (R Foundation for Statistical Computing, Vienna, Austria; <https://www.r-project.org/>). Continuous variables were analyzed using the independent two-sample t-test (parametric) or Mann-Whitney U test (non-parametric), while categorical variables were assessed via the chi-square test or Fisher's exact test, as appropriate. Univariate logistic regression was first applied to screen potential predictors, followed by multivariable logistic regression to identify independent risk factors. Receiver operating characteristic (ROC) curves and decision curve analysis (DCA) were generated using the "pROC" and "rmda" packages in R, respectively. The DeLong test was employed to compare the area under the curve (AUC) values across different models. A two-tailed P value < 0.05 was considered statistically significant.

Results

Clinical characteristics of patients

This study included a total of 174 patients, aged 28–83 years (mean age: 48.1 ± 10.2 years). Among them, 44 patients were diagnosed with ADH, 86 with intraductal papilloma, 5 with mucinous neoplasms, 4 with flat epithelial atypia, and 35 with sclerosing adenosis. Postoperative pathological examination revealed ductal carcinoma in situ (DCIS) or invasive ductal carcinoma (IDC) in 45 patients, resulting in an upgrade rate of 25.9% (45/174). A total of 174 patients were randomly allocated into a training cohort ($n = 121$, 70%) and a test cohort ($n = 53$, 30%) at a 7:3 ratio. There was no statistically significant difference in clinical and imaging features between the training and test sets ($P > 0.05$) (Tables 1 and 2).

Clinical and imaging model construction

Univariate logistic regression analysis was performed incorporating clinical and imaging features, with a threshold of $P < 0.1$ for initial screening. Three risk factors were identified: age, maximum lesion diameter, and BPE (Table 3). Variables that showed statistically significant differences in the univariate analysis were then included in multivariate logistic regression analysis, with a threshold set at $P < 0.05$. Ultimately, two independent risk factors were identified: age and BPE (Table 4). A clinical and imaging feature model was subsequently constructed based on these findings.

Table 1 Comparison of clinical and imaging characteristics of high-risk lesion patients in the training and test sets

n	Age (x ± s)	Maximum lesion diameter (mm, x ± s)	Menopause		Family history		Fibroglandular tissue		Clinical symptoms			TIC curve			BPE		Enhancement type	
			Yes	No	Yes	No	Dense	Non-dense	Pain	Nipple blood/fluid discharge	Palpable mass	Washout	plateau	Persistent	a/b	c/d	Mass	Non-mass
Training set	48.83 ± 10.67	27.88 ± 14.11	47	74	6	115	27	94	57	50	14	19	87	15	73	48	58	63
Test set	46.26 ± 8.80	26.58 ± 12.50	15	38	2	51	12	41	23	22	8	12	38	3	33	20	23	30
tX2	-1.54	-0.58	1.79	0.00	0.00	0.00	0.00	0.47	0.789	2.61	0.271	0.06	0.810	0.31	0.810	0.581		
P-value	0.126	0.564	0.181	1.000	0.962	0.962	0.789	0.271	0.810	0.581								

Model performance evaluation and comparison

The performance of the radiomic models based on the intratumoral, peritumoral 3 mm, peritumoral 5 mm, and peritumoral 7 mm regions was compared (Fig. 2A-B). The results demonstrated that the radiomic model incorporating intratumoral features exhibited superior diagnostic efficacy in predicting postoperative pathological upgrading (malignant transformation) of high-risk breast lesions, with AUC values of 0.791 and 0.781 for the training and test sets, respectively. The radiomic models based on the 3 mm, 5 mm, and 7 mm peritumoral features achieved AUC values of 0.704, 0.633, and 0.579, respectively, in the training set, and 0.654, 0.643, and 0.561 in the test set. Delong’s test revealed no statistically significant differences in AUC among the peritumoral regions. However, the peritumoral 3 mm model showed higher AUC values compared to the peritumoral 5 mm and 7 mm models. Consequently, the combined intratumoral-peritumoral model was developed by integrating the optimal 3 mm peritumoral radiomic features with intratumoral characteristics. This integrated model demonstrated robust predictive performance, achieving AUC values of 0.830 in the training cohort and 0.818 in the test cohort.

A triple-feature integrated model was developed by synergistically combining clinical and imaging predictors (selected through univariate and multivariate logistic regression analyses) with radiomic features derived from both intratumoral regions and 3 mm peritumoral expansions. In the training set, the combined model demonstrated the highest diagnostic performance (AUC=0.883), outperforming the clinical and imaging feature model (AUC=0.745, P=0.003), the intratumoral radiomic feature model (AUC=0.791, P=0.027), the peritumoral radiomic feature model (AUC=0.704, P=0.001), and the combined intratumoral and peritumoral radiomic model (AUC=0.830, P=0.004). In the test set, the combined model also showed the highest diagnostic performance (AUC=0.851). The specificity and accuracy of the combined model were higher than those of the other models in both the training and test sets (Fig. 2C-D). The nomogram constructed based on the combined model, the combined intratumoral and peritumoral Rad scores with clinical and imaging features, is shown in Fig. 3. The nomogram integrated radiomics signature, age, and BPE, demonstrating excellent discrimination.

Calibration curve analysis of the combined model (Fig. 4) revealed that the calibration curves, with the X-axis representing predicted probabilities and the Y-axis representing actual probabilities, showed a good fit with the 45° ideal line for both the training and test sets. The predicted probabilities of postoperative upgrades of high-risk breast lesions were consistent with the actual

Table 2 Comparison of MRI characteristics of high-risk lesion patients in the training and test sets

	<i>n</i>	TIC curve			BPE		Enhancement type	
		Palpable mass	Nipple blood/fluid discharge	Pain	a/b	c/d	Mass	Non-mass
Training set	121	19	87	15	73	48	58	63
Test set	53	12	38	3	33	20	23	30
<i>t/x2</i>		2.61			0.06		0.31	
<i>P-value</i>		0.271			0.81		0.581	

upgrade probabilities, with no significant deviation observed.

DCA (Fig. 5) demonstrated that the prediction model curves for both the training and test sets were superior to the two extreme lines. When the risk threshold was greater than 0.00, a net benefit could be achieved, facilitating clinical decision-making.

Discussion

The diagnosis of high-risk breast lesions currently relies predominantly on CNB, which serves as the clinical gold standard for histopathological assessment prior to surgical intervention. Due to variations in biopsy techniques and the amount of tissue sampled, the upgrade rate of high-risk lesions can vary significantly. According to the literature, the upgrade rate of high-risk lesions after surgical excision ranges from 9.9 to 35.1%. There is a substantial difference in upgrade rates among various histological subtypes: ADH has an upgrade rate of 0–62%, lobular carcinoma in situ (LCIS) ranges from 0 to 55%, and complex sclerosing adenosis ranges from 0–18% [3, 4]. In this study, the overall upgrade rate of high-risk lesions reached 25.9%.

Given the varying degrees of risk associated with high-risk lesions, corresponding clinical interventions and follow-up measures also differ. The development of treatment plans relies on the collaboration of a multidisciplinary team of clinicians, pathologists, and radiologists. In recent years, there has been ongoing debate regarding whether high-risk lesions should be surgically excised. Some scholars [18] argue that breast cancer tissue may be present around the biopsy site, and high-risk lesions carry the risk of upgrading to malignant lesions; therefore, surgical excision should be performed for high-risk lesions. Emerging evidence challenges the traditional surgical paradigm for high-risk breast lesions, as a significant proportion (up to 30%) of these lesions ultimately prove benign on postoperative histopathology. Recent studies have advocated for more conservative management strategies, such as vacuum-assisted biopsy/excision (VAB/E) or active surveillance protocols in select CNB-diagnosed high-risk lesions, thereby reducing overtreatment and avoiding unnecessary surgical interventions [16, 19].

While breast MRI has become a critical tool in diagnosing high-risk breast lesions, limited evidence exists

regarding its correlation with lesion upgrade outcomes [17]. Prior studies have established a link between BPE severity and estrogen-dependent fluctuations, particularly across menstrual phases [17, 20]. Notably, BPE levels may serve as a potential biomarker for breast cancer risk stratification [17, 20]. Expanding on these insights, You et al. [21] integrated multimodal data (mammography, MRI, and clinical parameters) to demonstrate that moderate-to-marked BPE on MRI independently predicts high-risk lesion upgrades in multivariate analyses. Consistent with these findings, our study further validated the prognostic significance of moderate-to-marked BPE as an independent risk determinant for lesion upgrade.

Current evidence on predictors of malignant upgrades in high-risk breast lesions remains limited. Historically, breast radiomic research has predominantly focused on intratumoral heterogeneity, largely overlooking the biologically rich and prognostically significant information embedded within the peritumoral microenvironment. The peritumoral region of breast tumors may contain important biological information that is difficult to detect through traditional imaging diagnosis, such as angiogenesis, lymphangiogenesis, peritumoral infiltration of blood vessels, and desmoplastic reactions [22].

The study [23] revealed that peritumoral imaging features within 0–3 mm surrounding the primary breast cancer lesion on MRI correlate with tumor-infiltrating lymphocyte (TIL) density, suggesting that peritumoral radiomic features may characterize the tumor microenvironment in breast cancer. Zhou et al. [24] segmented the intratumoral regions on DCE-MRI images from 133 patients with benign and malignant breast lesions. They expanded the intratumoral ROI by factors of 1.2, 1.5, and 2.0 to encompass peritumoral areas. Their findings demonstrated that the radiomics model incorporating small peritumoral regions (1.2×, 1.5×, 2.0× expansion) achieved the highest accuracy in distinguishing benign from malignant breast tumors. This highlights that combining intratumoral and limited peritumoral radiomic features outperforms models relying solely on intratumoral features. Lee et al. found that radiomic models based on intratumoral and peritumoral features derived from DCE-MRI images demonstrated high performance in differentiating benign and malignant breast lesions, and were comparable to radiologists' assessments [25]. Our prior investigation [26] was exclusively focused on

Table 3 Univariate analysis of high-risk lesion patients in the training set

n	Age (x ± s)	Maximum lesion diameter (mm, x ± s)	Menopause		Family history		Fibroglandular tissue		Clinical symptoms			TIC curve			BPE		Enhancement type	
			Yes	No	Yes	No	Dense	Non-dense	Palpable mass	Nipple blood/fluid discharge	Pain	Persistent	plateau	Washout	a/b	c/d	Mass	Non-mass
Training set	34	52.7 ± 11.2	14	20	3	31	8	26	13	17	4	6	25	3	13	21	20	14
Test set	87	47.3 ± 10.1	33	54	3	84	19	68	44	33	10	13	62	25	60	27	38	49
tX2		-2.55	0.11	0.58	0.448	0.841		1.65	0.437	0.62	0.734		9.65	2.25				
P-value		0.012	0.742												0.002		0.134	

radiomic feature extraction from a fixed 5 mm peritumoral margin, whereas emerging evidence suggests significant spatial heterogeneity in biological processes (e.g., angiogenesis, immune infiltration) across differentially expanded peritumoral regions. This biological gradient may critically influence malignant transformation risk stratification, underscoring the necessity of systematic multi-margin analyses to decode microenvironmental dynamics. These findings suggest that the peritumoral region has potential diagnostic value. Therefore, in this study, we systematically evaluated peritumoral regions at incremental expansions of 3 mm, 5 mm, and 7 mm from the tumor boundary to extract and analyze radiomic features, aiming to identify the optimal peritumoral margin for predicting malignant upgrades in high-risk lesions. The results demonstrated that the radiomic model based on the 3 mm peritumoral region achieved superior diagnostic performance compared to models using larger peritumoral margins (5 mm and 7 mm), with an AUC of 0.704. Potential underlying mechanisms merit consideration. First, signal dilution may occur as radiomic features extracted from 5 to 7 mm perilesional margins incorporate non-specific signals from adjacent normal glandular tissue and vasculature, thereby compromising discriminative power for lesion characterization. Second, excessive spatial smoothing introduced by wide-margin delineation increases volumetric averaging effects, which obscures fine-scale heterogeneity—a critical biomarker for risk stratification that reflects subvoxel architectural distortions associated with early malignant transformation.

Thus, we ultimately combined the intratumoral radiomic features with the highest-performing peritumoral 3 mm radiomic features. The results demonstrated that the integrated model combining intratumoral radiomic features, 3 mm peritumoral radiomic signatures, along with clinical and imaging predictors achieved the highest diagnostic performance in the training cohort, with an AUC of 0.883. The combined model demonstrated superior performance compared to models based solely on clinical and imaging features, intratumoral radiomics, peritumoral radiomics, or even the combination of intratumoral and peritumoral radiomics. In the test cohort, the integrated model achieved the highest diagnostic accuracy, with an AUC of 0.851. By synergistically incorporating intratumoral and peritumoral radiomic features derived from breast DCE-MRI with clinical and imaging predictors, this multimodal framework not only optimizes diagnostic precision but also provides actionable imaging-based evidence and establishes a nomogram to guide personalized clinical decisions. It addresses two clinical challenges: avoiding unnecessary biopsies in low-risk BI-RADS 4 lesions and

Table 4 Univariate and multivariate logistic regression analysis in the training set

	Univariate					Multivariate				
	β	S.E	Z	OR(95%CI)	P-value	β	S.E	Z	OR(95%CI)	P-value
Age	0.05	0.02	2.41	1.05(1.01~1.09)	0.016	0.05	0.03	2.05	1.06(1.01~1.11)	0.040
Maximum lesion diameter	0.05	0.02	3.23	1.05(1.02~1.08)	0.001	0.03	0.02	1.43	1.03(0.99~1.07)	0.154
BPE	1.28	0.42	3.03	3.59(1.57~8.21)	0.002	1.45	0.56	2.62	4.28(1.44~12.74)	0.009
Rad score	1.00	0.21	4.68	2.72(1.79~4.13)	<0.001	1.01	0.24	4.19	2.75(1.71~4.41)	<0.001

Abbreviations: OR: odds ratio; CI: confidence interval; Rad scores: radiomics score; S.E: standard deviation

Note: β : regression coefficient

Key findings: Age, BPE, and Rad score demonstrated statistically significant associations in multivariate analyses, establishing them as core independent predictors. BPE exhibited the highest odds ratio, suggesting its clinical relevance may surpass that of the radiomics score. Furthermore, Rad score retained statistical significance in both univariate and multivariate models, reinforcing its validity as a robust quantitative biomarker for breast cancer risk stratification

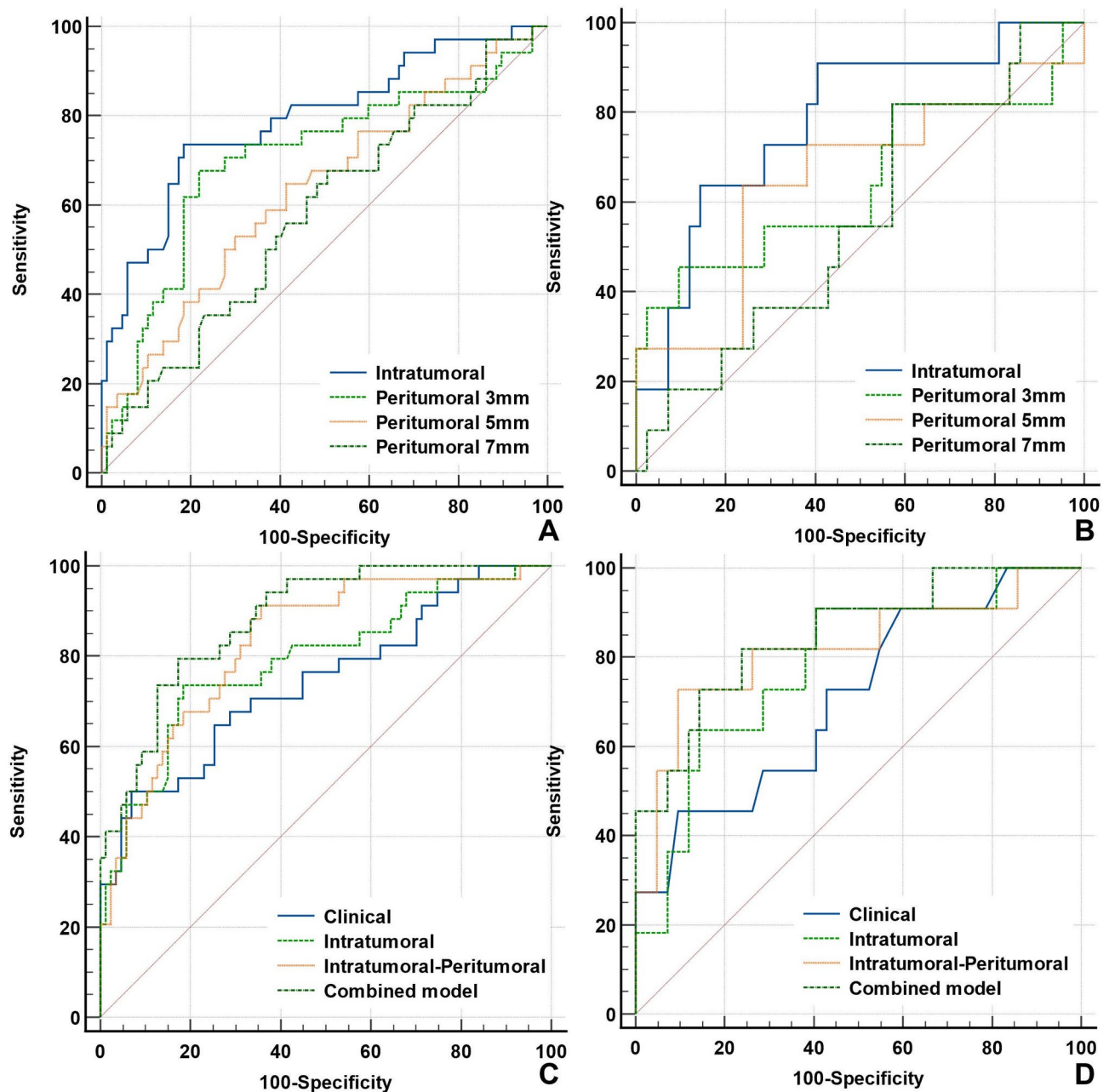


Fig. 2 ROC curves of intratumoral and peritumoral radiomics models in the training set (A, C) and test set (B, D)

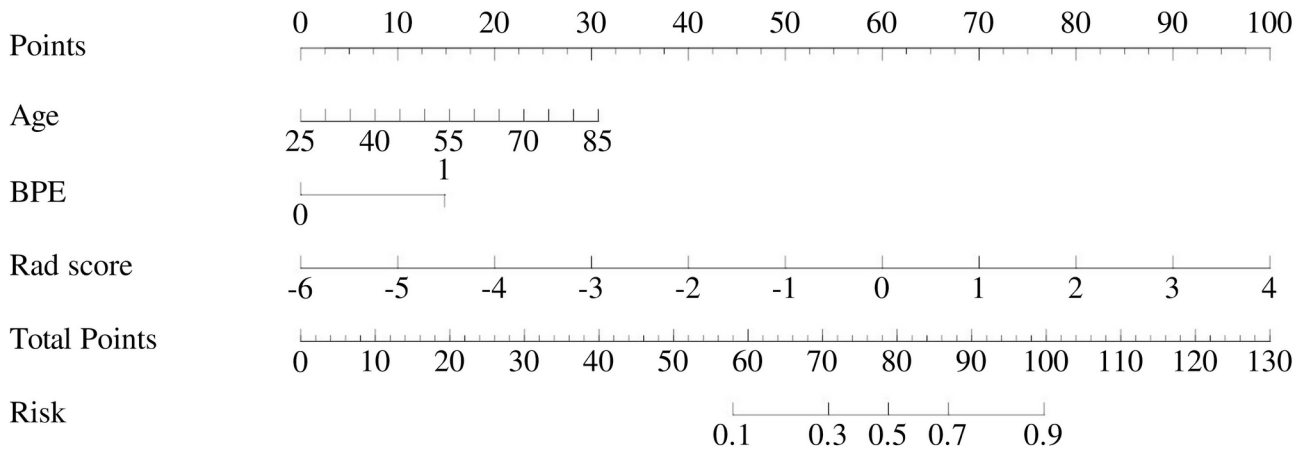


Fig. 3 Nomogram constructed from clinical and radiomics features combined with intratumoral and peritumoral radiomics features

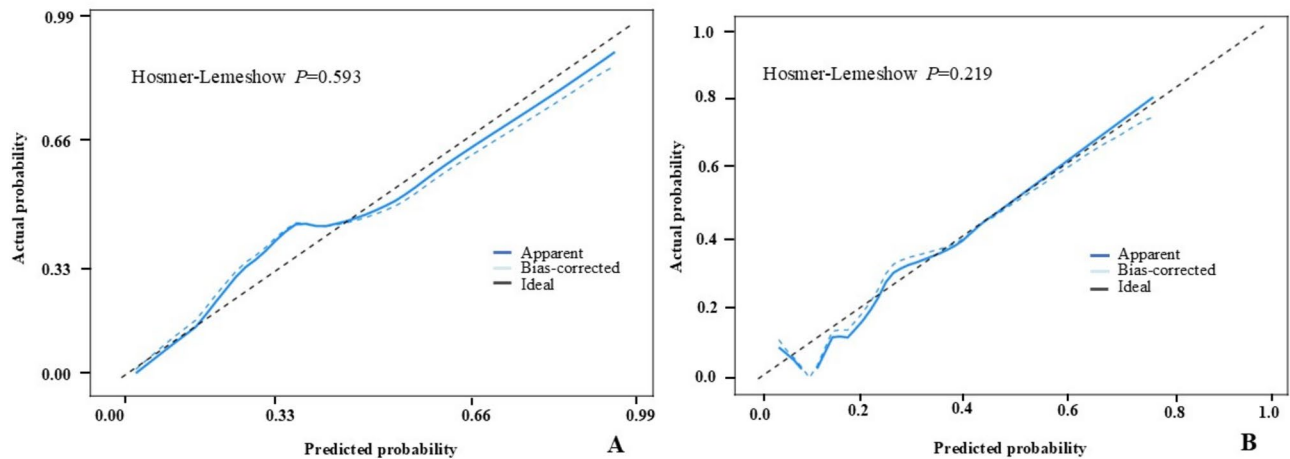


Fig. 4 Calibration curves of the combined model (Clinical, intratumoral, and peritumoral features) in the training and test sets

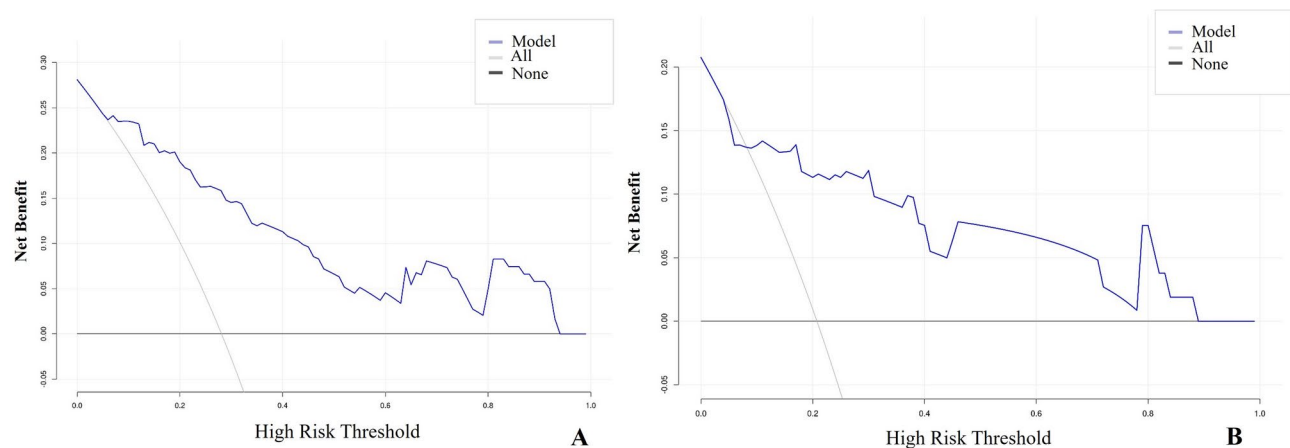


Fig. 5 Decision curve analysis of the combined prediction model in the training and test sets

prioritizing high-risk cases for immediate intervention, effectively reducing healthcare costs and patient anxiety.

This study has several limitations. First, its mono-centric retrospective design may limit generalizability

to diverse populations and imaging protocols. Second, radiomic features are sensitive to MRI scanner variability and acquisition parameters. Although intensity normalization was applied, future multi-center studies

should adopt ComBat harmonization or deep learning-based image synthesis to mitigate scanner effects. Third, manual tumor segmentation, particularly for peritumoral regions, may introduce inter-observer variability.

Conclusion

This combination prediction model combines intratumoral and peritumoral radiomic features with clinical and imaging data, demonstrating strong diagnostic performance in predicting the pathological progression of high-risk breast lesions. This approach can better stratify and treat high-risk lesions.

Acknowledgements

The authors would like to thank all those involved in the study for dedicating their time and skills to the completion of this study. This paper is supported by Shenzhen Science and Technology Research and Development Fund [Grant Number GJHZ20220913142613025], which was critical to the successful completion of this study.

Author contributions

All authors contributed to the conception and design of the study. Yuting Yang and Tingting Liao wrote the first draft of the manuscript, and all authors commented on the manuscript's early versions. Xiaohui Lin and Rushan Ouyang provided major critical reviews of the intellectual content of the article. Yuting Yang, Tingting Liao and Qiu Chen conducted material preparation and data analysis. All authors read and approved the final manuscript, and Jie Ma provided administrative and financial support.

Funding

This study was supported by the Shenzhen Science and Technology Research and Development Fund (GHSZ20210705142208024).

Data availability

The datasets generated during and/or analyzed during the current study are not publicly available due to the privacy of hospital data. However, they are available from the corresponding author upon reasonable request.

Declarations

Ethics approval and consent to participate

This study was approved by the Ethics Committee of Shenzhen Hospital (LL-KY-2021624). This study was conducted under the Declaration of Helsinki.

Consent for publication

Not applicable.

Competing interests

The authors declare no competing interests.

Clinical trial number

Not applicable.

Author details

¹Department of Radiology, Shenzhen People's Hospital, The Second Clinical Medical College of Jinan University, Shenzhen 518020, China

²Department of Radiology, The Eighth Affiliated Hospital of Sun Yat-sen University, Shenzhen 528406, China

³Department of Ultrasound, The Second Affiliated Hospital of Guangzhou Medical University, Guangzhou, China

Received: 19 February 2025 / Accepted: 15 April 2025

Published online: 06 May 2025

References

- Bray F, Laversanne M, Sung H, Ferlay J, Siegel RL, Soerjomataram I et al. Global cancer statistics 2022: GLOBOCAN estimates of incidence and mortality worldwide for 36 cancers in 185 countries [J]. *CA: A Cancer Journal for Clinicians*, 2024, 74(3): 229–63. DOI:10.3322/caac.21834.
- Rubio IT, Wyld L, Marotti L, Athanasiou A, Regitnig P, Catanuto G et al. European guidelines for the diagnosis, treatment and follow-up of breast lesions with uncertain malignant potential (B3 lesions) developed jointly by EUSOMA, EUSOBI, ESP (BWG) and ESSO [J]. *Eur J Surg Oncol*, 2024, 50(1): 107292. DOI:10.1016/j.ejso.2023.107292.
- El-Sayed ME, Rakha EA, Reed J, Lee AH, Evans AJ, Ellis IO. Predictive value of needle core biopsy diagnoses of lesions of uncertain malignant potential (B3) in abnormalities detected by mammographic screening [J]. *Histopathology*, 2008, 53(6): 650–7. DOI:10.1111/j.1365-2559.2008.03158.x.
- Mooney KL, Bassett LW, Apple SK. Upgrade rates of high-risk breast lesions diagnosed on core needle biopsy: a single-institution experience and literature review [J]. *Mod Pathol*, 2016, 29(12): 1471–84. DOI:10.1038/modpathol.2016.127.
- Elkenawy EM, Alhussan AA, Khafaga DS, Tarek Z, Elshewey AM. Greylag goose optimization and multilayer perceptron for enhancing lung cancer classification [J]. *Sci Rep*, 2024, 14(1): 23784. DOI:10.1038/s41598-024-72013-x.
- Zhang H, Zhao T, Ding J, Wang Z, Cao N, Zhang S et al. Differentiation between invasive ductal carcinoma and ductal carcinoma in situ by combining intratumoral and peritumoral ultrasound radiomics [J]. *Biomed Eng Online*, 2024, 23(1): 117. DOI:10.1186/s12938-024-01315-y.
- Wang X, Wei M, Chen Y, Jia J, Zhang Y, Dai Y et al. Intratumoral and peritumoral MRI-based radiomics for predicting extrapelvic peritoneal metastasis in epithelial ovarian cancer [J]. *Insights Imaging*, 2024, 15(1): 281. DOI:10.1186/s13244-024-01855-w.
- Urso L, Manco L, Cittanti C, Adamantiadis S, Szilagyi KE, Scribano G et al. (18) F-FDG PET/CT radiomic analysis and artificial intelligence to predict pathological complete response after neoadjuvant chemotherapy in breast cancer patients [J]. *Radiol Med*, 2025. DOI:10.1007/s11547-025-01958-4.
- Urso L, Quartuccio N, Caracciolo M, Evangelista L, Schirone A, Frassoldati A et al. Impact on the long-term prognosis of FDG PET/CT in luminal-A and luminal-B breast cancer [J]. *Nucl Med Commun*, 2022, 43(2): 212–9. DOI:10.1097/mnm.0000000000001500.
- Kettunen T, Okuma H, Auvinen P, Sudah M, Tiainen S, Sutela A et al. Peritumoral ADC values in breast cancer: region of interest selection, associations with hyaluronan intensity, and prognostic significance [J]. *Eur Radiol*, 2020, 30(1): 38–46. DOI:10.1007/s00330-019-06361-y.
- Wu PQ, Guo FL, Wang J, Gao Y, Feng ST, Chen SL et al. Development and validation of a dynamic contrast-enhanced magnetic resonance imaging-based habitat and peritumoral radiomic model to predict axillary lymph node metastasis in patients with breast cancer: a retrospective study [J]. *Quant Imaging Med Surg*, 2024, 14(12): 8211–26. DOI:10.21037/qims-24-558.
- Wang F, Cheng M, Du B, Li J, Li L, Huang W et al. Predicting microvascular invasion in small (≤ 5 cm) hepatocellular carcinomas using radiomics-based peritumoral analysis [J]. *Insights Imaging*, 2024, 15(1): 90. DOI:10.1186/s13244-024-01649-0.
- Yang J, Liu Y, Liu X, Wang Y, Wang X, Ai C et al. MRI-based intratumoral and peritumoral radiomics for assessing deep myometrial invasion in patients with early-stage endometrioid adenocarcinoma [J]. *Front Oncol*, 2024, 14: 1474427. DOI:10.3389/fonc.2024.1474427.
- Mo S, Luo H, Wang M, Li G, Kong Y, Tian H et al. Machine learning radiomics based on intra and peri tumor PA/US images distinguish between luminal and non-luminal tumors in breast cancers [J]. *Photoacoustics*, 2024, 40: 100653. DOI:10.1016/j.pacs.2024.100653.
- Liu Z, Hong M, Li X, Lin L, Tan X, Liu Y. Predicting axillary lymph node metastasis in breast cancer patients: A radiomics-based multicenter approach with interpretability analysis [J]. *Eur J Radiol*, 2024, 176: 111522. DOI:10.1016/j.ejrad.2024.111522.
- Giannotti E, James JJ, Chen Y, Sun R, Karuppiah A, Yemm J et al. Correction to: Effectiveness of percutaneous vacuum-assisted excision (VAE) of breast lesions of uncertain malignant potential (B3 lesions) as an alternative to open surgical biopsy [J]. *Eur Radiol*, 2022, 32(1): 742. DOI:10.1007/s00330-021-08157-5.
- Hu N, Zhao J, Li Y, Fu Q, Zhao L, Chen H et al. Breast cancer and background parenchymal enhancement at breast magnetic resonance imaging: a meta-analysis [J]. *BMC Med Imaging*, 2021, 21(1): 32. DOI:10.1186/s12880-021-00566-8.

18. Ring NY, Diflorio-Alexander RM, Bond JS, Rosenkranz KM, Cervantes E, Sohn JH et al. Papillary and sclerosing lesions of the breast detected and biopsied by MRI: Clinical management, upgrade rate, and association with apocrine metaplasia [J]. *Breast J*, 2019, 25(3): 393–400. DOI.10.1111/tbj.13238.
19. Pinder P S E, Shaaban A, Deb R, Desai A, Gandhi A, Lee L A H S, et al. NHS breast screening multidisciplinary working group guidelines for the diagnosis and management of breast lesions of uncertain malignant potential on core biopsy (B3 lesions). *Clin Radiol*. 2018;73(8):682–92. <https://doi.org/10.1016/j.crad.2018.04.004>.
20. Liu K, Liu Q, Xu F, Zhang CX, Zhang YL. The clinical value of X-ray and background enhanced features by MRI in prediction of diagnosis upgrade in breast High-Risk benign lesions [J]. *Med Theory Pract*. 2023;36(6):919–2128. <https://doi.org/10.19381/j.issn.1001-7585.2023.06.006>.
21. You C, Peng WJ, Gu YJ, Chen S, Liu XH, Jiang TT et al. The diagnostic value of both mammography and MRI in combination with clinical features in Highrisk breast lesions [J]. *Chin J Radiol*, 020, 54(03): 203–8. <https://doi.org/10.3760/cma.j.issn.1005-1201.2020.03.006>
22. Yu H, Meng X, Chen H, Han X, Fan J, Gao W et al. Correlation Between Mammographic Radiomics Features and the Level of Tumor-Infiltrating Lymphocytes in Patients With Triple-Negative Breast Cancer [J]. *Front Oncol*, 2020, 10: 412. DOI.10.3389/fonc.2020.00412.
23. Braman N, Prasanna P, Whitney J, Singh S, Beig N, Etesami M et al. Association of Peritumoral Radiomics With Tumor Biology and Pathologic Response to Preoperative Targeted Therapy for HER2 (ERBB2)-Positive Breast Cancer [J]. *JAMA Netw Open*, 2019, 2(4): e192561. DOI.10.1001/jamanetworkopen.2019.2561.
24. Zhou J, Zhang Y, Chang KT, Lee KE, Wang O, Li J et al. Diagnosis of Benign and Malignant Breast Lesions on DCE-MRI by Using Radiomics and Deep Learning With Consideration of Peritumor Tissue [J]. *J Magn Reson Imaging*, 2020, 51(3): 798–809. DOI.10.1002/jmri.26981.
25. Lee HJ, Nguyen AT, Ki SY, Lee JE, Do LN, Park MH et al. Classification of MR-Detected Additional Lesions in Patients With Breast Cancer Using a Combination of Radiomics Analysis and Machine Learning [J]. *Front Oncol*, 2021, 11: 744460. DOI.10.3389/fonc.2021.744460.
26. Liao T, Yang Y, Lin X, Ouyang R, Deng Y, Ma J. High-risk breast lesions: a combined intratumoral and peritumoral radiomics nomogram model to predict pathologic upgrade and reduce unnecessary surgical excision [J]. *Front Oncol*, 2024, 14: 1479565. DOI.10.3389/fonc.2024.1479565.

Publisher's note

Springer Nature remains neutral with regard to jurisdictional claims in published maps and institutional affiliations.